Evaluation of the weld bead homogeneity obtained by laser welding with powder addition in duplex steel UNS S32304 through images acquired by micro-CT

Xavier, G. C.[1]*; Alves, H. D. L.[2]; Orlando, M. T. D.[1]

[1] Postgraduate Program in Mechanical Engineering, Federal University of Espírito Santo, Vitória, ES, Brazil.
[2] Department of Nuclear Engineering, Federal University of Rio de Janeiro, Rio de Janeiro, RJ, Brazil.

* e-mail: gabriel.xavier@edu.ufes.br

Resumo

Os aços inoxidáveis duplex se caracterizam pela presença de duas fases (ferrita e austenita) que idealmente devem estar presentes em igual proporção no material. São amplamente utilizados em indústrias como nuclear, química, petroquímica e óleo e gás offshore devido à sua alta resistência à corrosão e resistência mecânica. Durante a soldagem desses materiais, é necessário controlar cuidadosamente as taxas de resfriamento para manter a proporção adequada de ferrita-austenita e evitar a formação de precipitados indesejáveis. A soldagem a laser, devido à sua alta energia e altas taxas de resfriamento, é vantajosa para produzir zonas termicamente afetadas limitadas e prevenir a formação de precipitados indesejáveis. Diante desse contexto, o presente trabalho objetivou avaliar a homogeneidade de cordões de solda obtidos por soldagem a laser utilizando o pó do aço duplex UNS S32304 em chapas de aço inoxidável do mesmo material a partir de imagens obtidas pelo ensaio de microtomografia. Baseando-se na premissa de que há uma forte correlação entre a intensidade da cor verde e a presença da ferrita na amostra e entre o vermelho e a presença da austenita nas fotografias transversais dos cordões de solda obtidas da microtomografia, o trabalho propõe estabelecer curvas matemáticas de ajuste que modelam a quantificação de cada fase típica do duplex pela intensidade do pixel RGB. Como resultado, nota-se que o melhor ajuste para o comportamento esperado da proporção da fase por intensidade de pixel obtido para a fase ferrítica (exponencial) é diferente da curva obtida para a austenita (logarítmica). Essa diferença foi atribuída à diferença de temperatura para formação e da cinética de formação de cada fase. Além disso, verificamos que a amostra soldada na presença do pó metálico apresentou um cordão de solda mais homogêneo, sendo nítida a diferenciação entre a zona fundida e a zona termicamente afetada quando comparada com a imagem obtida do cordão de solda autógeno. Por fim, observou-se a existência de um ruído expressivo no resultado da composição de fases pelo ensaio de microtomografia na austenita quando comparado com o ruído proveniente da fase ferrítica, que foi atribuído ao fato da austenita estar localizada preferencialmente na região de contorno de grão da ferrita, além de estar presente em baixa proporção no cordão quando comparada com a fase ferrítica.

Abstract

Duplex stainless steels are widely used in industries such as nuclear, chemical, petrochemical, and offshore oil and gas due to their high corrosion resistance and mechanical strength. They are characterized by the presence of two phases (ferrite and austenite) that ideally should be in equal proportion in the material. During the welding of these materials, it is necessary to carefully control the cooling rates to maintain the proper proportion of ferrite-austenite and avoid the formation of undesirable precipitates. Laser welding, due to its high energy and high cooling rates, is advantageous in producing limited heat-affected zones and preventing the formation of undesirable precipitates. In this context, the present work aimed to evaluate the homogeneity of weld beads obtained by laser welding using duplex stainless steel powder (UNS S32304) on stainless steel sheets of the same material, based on images obtained through microtomography testing. Based on the premise that there is a strong correlation between the intensity of the green color and the presence of ferrite in the sample, as well as between the red color and the presence of austenite in the cross-sectional photographs of the weld beads obtained from micro-CT, the study proposed to establish mathematical fitting curves that model the quantification of each typical phase of the duplex by the intensity of the RGB pixel. As a result, it was observed that the best fit for the expected behavior of phase proportion by pixel intensity obtained for the ferritic phase (exponential) is different from the curve obtained for austenite (logarithmic). This difference was attributed to the difference in temperature for formation and the kinetics of formation for each phase. In addition, it was found that the sample welded in the presence of the metallic powder exhibited a more homogeneous weld bead, with a clear differentiation between the fusion zone and the heat-affected zone. Finally, it was observed that there was a significant noise in the result of phase composition by micro-CT testing for austenite compared to the noise in the ferritic phase. This was attributed to the fact that austenite is primarily located in the grain boundary region of ferrite and is present in a lower proportion in the weld bead compared to the ferritic phase.

Keywords: Duplex stainless steel, laser welding, micro-CT, weld bead homogeneity, RGB intensity.

1. Introduction

Duplex stainless steels are characterized by the presence of two phases, ferrite (α) and austenite (γ), which ideally should be present in equal proportions in the material.

This class of materials is widely utilized in corrosive environments, such as nuclear, chemical, petrochemical, pulp and paper, power generation, and oil and gas industries, owing to their remarkable combination of high corrosion resistance and mechanical strength [1]. The low manufacturing cost, high processing efficiency, and wide availability of different types of powders enhance the demand for sintered stainless steel [2-5].

Figure 1 presents a schematic ternary phase diagram (iron-chromium-nickel) for a steel with 68% Fe, which helps to understand the metallurgical behavior for the formation of both typical phases in a duplex steel.

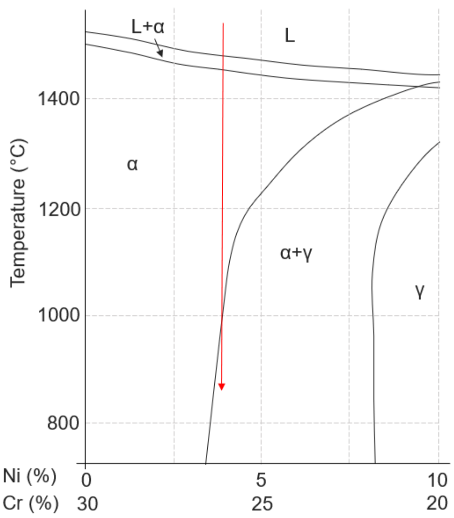

Figure 1: Schematic ternary phase diagram Fe-Cr-Ni for an alloy with 68% Fe.

According to Figure 1, the red line shows the cooling behavior of an alloy with approximately 4% nickel from the liquid phase. It can be observed that solidification concludes in the purely ferritic phase (above 1400 °C). The beginning of austenite formation only occurs when the temperature reaches a value close to 1000 °C, as the temperature decreases. Thus, the phase transformation sequence for the formation of both phases in the duplex during cooling can be simplified as: L→L+α→α→α+γ. Austenite initially forms in the region of ferritic grain boundaries and can advance into the interior of the grains in a morphology known as Widmanstätten. [6].

The fabrication of components using duplex steels generally requires welding operations. However, welding this class of materials poses a significant challenge related to controlling the cooling rate. It cannot be too high to alter the ideal proportion of ferrite and austenite in the weld bead, nor too slow to induce the formation of intermetallic precipitates that could weaken the material [7,8]. Laser welding offers several advantages compared to other techniques, such as higher precision, lower cost, and a higher cooling rate, resulting in a finer structure and increased tensile strength [9-11].

The microCT technique is a powerful tool for detecting discontinuities in weld beads, such as cracks and porosity. Several studies have demonstrated the positive results of applying a post-processing methodology on 3D images using this technique [12,13].

Therefore, the present work aims to evaluate the homogeneity of weld bead obtained by laser welding using duplex stainless steel powder UNS S32304 on sheets of the same duplex stainless steel based on images obtained through microCT testing.

2. Methodology

The manufacturing of the duplex powder followed the top-down technology, with mechanical grinding of the steel plate using a diamond mill with a contact pressure of 8 x 10^4 Pa at a temperature of 90 K [14], carried out at the Photonics Nanometry Laboratory of the Department of Mechanical Engineering at Federal University of Espírito Santo. Laser welding on the rolled duplex stainless steel sheets UNS S32304 with dimensions of 100 x 72 mm² was performed at ISF, RWTH, in Germany using the FOCUS LaVa L95 equipment. The beam generator used was the Trumpf Multimode laser, model TruDisk 16002 with a wavelength of 1030 nm and a fiber diameter of 200 nm. In all welding processes, a working pressure of 1 mbar and argon with a flow rate of 0.5 ln/min were used as the shielding gas. For autogenous welding, the working power was set to 420 W, with a speed of 300 mm/min and a zero focal beam distance.

Two welded samples were fabricated: autogenous and laser-welded with metallic powder (UNS S32304). All samples underwent X-ray diffraction technique to obtain phase quantification and microCT analysis to assess the homogeneity of the weld bead.

The X-ray diffraction technique was performed at the Photonics Nanometry Laboratory of the Department of Mechanical Engineering at Federal University of Espírito Santo using a Bragg-Brentano geometry diffractometer, equipped with a 185mm diameter goniometer, a 0.02-degree step and a graphite monochromator. The microCT test was performed using the CoreTOM equipment from TESCAN, located at the Enhanced Oil Recovery Laboratory (LRAP) at the Federal University of Rio de Janeiro - UFRJ. The X-ray source used has a variable voltage between 30 and 230 kV and a maximum power of 300 W. The X-ray detector was a flat panel (amorphous Si) with a matrix of 2856 × 2856 pixels. The maximum spatial resolution of the equipment is 3 µm.

From the three-dimensional images generated in the microCT test, a transverse photograph of the weld bead region is obtained using the ImageJ® software. Subsequently, the y(x) function, which represents the RGB pixel intensity (ranging from 0 to 255) for each sample as a function of the distance from a horizontal line passing through the center of each image, was obtained using the same software.

Based on the premise that there is a strong correlation between the intensity of the green color and the presence of ferrite in the sample and between the red color and the presence of austenite, a methodology was defined, as presented in Figure 2, to obtain the z(x) function, which represents the phase proportion along the horizontal line of each sample.

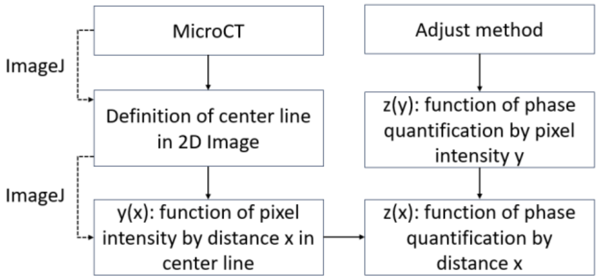

Figure 2: Methodology adopted to obtain the function z(x), which represents the quantification of phase by the horizontal distance defined in the center line of the image obtained from the microCT test.

Hence, an adjustment methodology was necessary to determine the z(y) function, which represents the phase quantification based on pixel intensity. Thus, Table 1 shows the mathematical functions (linear, exponential, and logarithmic) that were used in this adjustment step to model the described physical phenomenon.

Table 1 - Mathematical functions used in the fitting step to correlate the physical model of phase quantification with pixel intensity.

Adjust	Function z(y)	Coefficient
Linear	$b_0 \cdot y + \frac{z(y_{max})}{y_{max}}$	b_0
Exponential	$z(y_{max}) \cdot (1 - e^{-b_1 \cdot y})$	b_1
Logarithmic	$\log(b_2 \cdot y)$	b_2

Regarding Table 1, y_{max} corresponds to the maximum pixel intensity value recorded in the phase for each sample and $z(y_{max})$ represents the proportion of the phase at the maximum pixel intensity, which is the region where the highest proportion of the phase is expected, such as the fused zone (FZ) region for ferrite and the base metal (BM) region for the austenitic phase. The coefficients b_0, b_1, and b_2 are calculated considering the initial boundary condition (x=0), which is known. The y(x) function in the initial state (y_0) represents the first pixel value of the y(x) function obtained from the microCT test image, while the initial state of the z(x) function, z_0, represents the expected phase quantification for the base metal (BM) region of the samples, based on the proportion of the phase in the received plate.

3. Discussion of results

Table 2 shows the result of phase quantification obtained by X-ray for the ferritic phase.

Table 2 - Result of ferritic phase quantification by XRD.

Sample	Average	Deviation	Min	Max
Sheet as received	59%	6%	53%	65%
Autogenous	69%	7%	62%	76%
Powder	78%	8%	70%	86%

Table 3 shows the result of phase quantification obtained by X-ray for the austenitic phase.

Table 3 - Result of austenite phase quantification by XRD.

Sample	Average	Deviation	Min	Max
Sheet as received	41%	6%	37%	45%
Autogenous	31%	3%	28%	34%
Powder	15%	2%	13%	17%

Tables 4 and 5 present the values of pixel intensity y_0 and y_{max} obtained from microCT analysis, as well as the coefficients (b_0, b_1, and b_2) calculated for each sample for ferrite and austenite, respectively.

Table 4 - Result of values of pixel intensity obtained from microCT analysis, as well as the coefficients (b0, b1, and b2) for ferritic phase.

Sample	y_0	y_{max}	b_0	b_1	b_2
Aut.	157	238	$2.1 \cdot 10^{-3}$	$9.5 \cdot 10^{-3}$	$2.5 \cdot 10^{-2}$
Powder	93	251	$1.7 \cdot 10^{-3}$	$1.3 \cdot 10^{-2}$	$4.2 \cdot 10^{-2}$

Table 5 - Result of values of pixel intensity obtained from microCT analysis, as well as the coefficients (b0, b1, and b2) for austenitic phase.

Sample	y_0	y_{max}	b_0	b_1	b_2
Aut.	186	214	$1.4 \cdot 10^{-3}$	$1.3 \cdot 10^{-2}$	$1.4 \cdot 10^{-2}$
Powder	211	245	$1.2 \cdot 10^{-3}$	$1.2 \cdot 10^{-2}$	$1.2 \cdot 10^{-2}$

Figure 3 presents the result of the function z(x) for autogenous sample for each tested function z(y) (linear, exponential, and logarithmic). The dashed lines represent the minimum and maximum limits for the phase quantification values obtained from the phase quantification analysis by X-ray diffraction (Table 2 and Table 3).

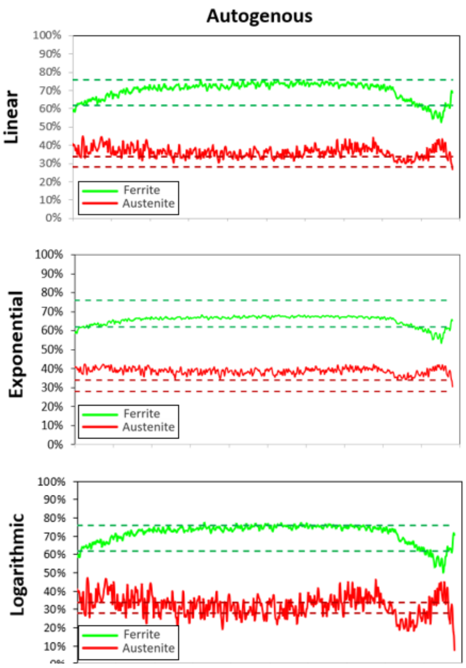

Figure 3: Phase quantification as a function of the horizontal distance for autogenous sample for each tested function z(y).

Figure 4 represents the same result shown previously for the sample welded with metallic filler powder.

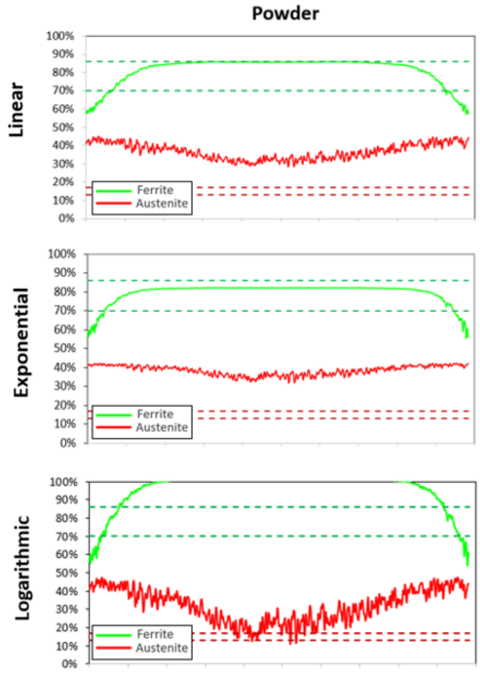

Figure 4: Phase quantification as a function of the horizontal distance for autogenous sample for each tested function z(y).

A qualitative comparison matrix was created to determine the best mathematical fit of z(y) among those analyzed for each phase. A score of 0, 1, or 2 was assigned to indicate a result identified as poor, medium, or good, respectively, based on the deviation obtained from the phase quantification analysis by DRX in Table 2 and Table 3 (dashed lines). When the curve is very close to the upper or lower limit, it is considered a "medium" score. The results are shown in Tables 6 for ferrite and Table 7 for austenite.

Table 6 - Result of the comparison method for ferrite.

Function	Aut	Powder	Score
Linear	Good	Medium	3
Exponential	Good	Good	4
Logarithmic	Medium	Poor	1

Table 7 - Result of the comparison method for austenite.

Function	Aut	Powder	Score
Linear	Poor	Poor	0
Exponential	Poor	Poor	0
Logarithmic	Good	Medium	3

Based on the results shown in Table 6 and Table 7, it is noted that the best fit for the expected behavior of phase proportion based on pixel intensity obtained for the ferritic phase (exponential) is different from the curve obtained for austenite (logarithmic). This is due to the difference in temperature for formation and the kinetics of formation for each phase. Solidification concludes in the ferritic phase and, as the temperature decreases, the formation of austenite occurs [6].

Finally, Figure 5 presents the result of the z(x) function, which represents the quantification of ferritic phase (green) and austenitic phase (red) as a function of the distance defined by the center line used as a reference for the analysis of the microCT test result, considering the best function z(y) obtained for each phase.

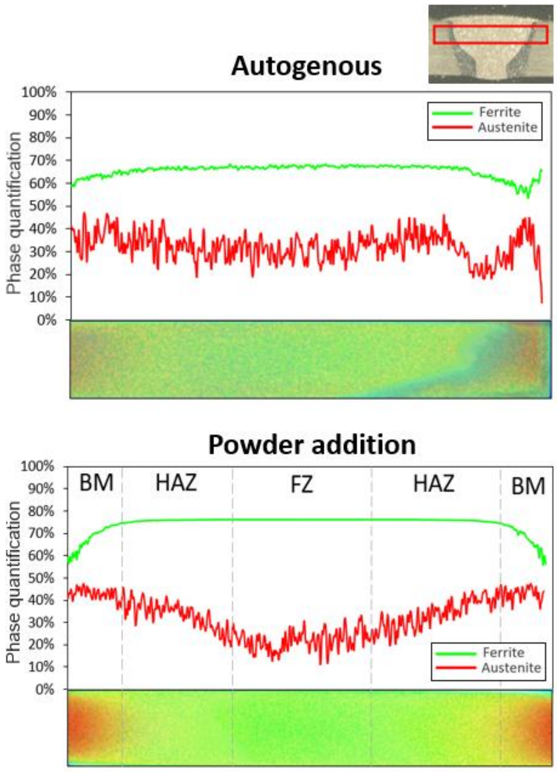

Figure 5 - Comparison between the quantification of the ferritic phase (green) and austenitic phase (red) based on the fitting of the images obtained in the MicroCT test of laser-welded samples.

According to Figure 5, it can be observed that the samples welded in the presence of powder exhibited a more homogeneous weld bead with a clear differentiation between the fusion zone (FZ) and the heat-affected zone (HAZ) when compared to the image obtained from the autogenous weld bead. Furthermore, significant noise is observed in the MicroCT test result for the austenitic phase compared to the noise from the ferritic phase. This is due to the nucleation and growth kinetics of austenitic grains in the ferritic matrix of the duplex steel alloy during cooling. The fact that austenite is preferentially located in the grain boundary region of ferrite, which is a high-energy region, and is present in a lower proportion, explains the higher noise in the signal and the difficulty in detecting this phase in the weld bead.

4. Conclusion

This study proposed two different mathematical models that describe the effect of phase proportion based on pixel intensity resulting from imaging analysis of a weld bead region on a duplex steel substrate. This behavior was described by an exponential function for ferrite and a logarithmic function for austenite. Additionally, laser welding using the duplex powder appears to be a promising technique considering the homogeneity of the weld bead when compared to autogenous welding.

6. Acknowledgements

The authors would like to thank CAPES, FAPES and CNPQ for the financial support provided.

7. References

[1] GUNN, R. N. Duplex stainless steel Microestructure, properties and application. [S.I.] 1997. ISBN: 9781855733183;

[2] OLIVEIRA, J. F. S. Estudos da Influência da Configuração em Compósitos Poliméricos Híbridos. Dissertação (Mestrado em Engenharia Mecânica), Programa de Pós-graduação em Engenharia Mecânica, Universidade Federal do Rio Grande do Norte – UFRN, Natal, 2007;

[3] CAMPBELL, F.C. Structural Composite Materials. [S.I.] Ohio: ASM International, 2010;

[4] OKE, S.R.; IGE, O.O.; FALODUN, O.E.; OKORO, A.M.; MPHAHLELE, M.R.; OLUBAMBI, P.A. Powder metallurgy of stainless steels and composites: a review of mechanical alloying and spark plasma sintering. The International Journal of Advanced Manufacturing Technology, v. 102, p. 3271–3290, 2019;

[5] BASAK, A.K.; PRAMANIK, A.; ISLAM, M.N.; ANANDAKRISHNAN, V. Challenges and recent developments on nanoparticle-reinforced metal matrix composites. Fillers and Reinforcements for Advanced Nanocomposites, Woodhead Publishing Series in Composites Science and Engineering, p. 349-367, 2015;

[6] ARMAS, Iris Alvarez; DEGALAIX, Suzanne Moreuil. Duplex stainless steels. [S.I.], 2009;

[7] CAETANO, G. A. Estudo do Comportamento Mecânico em Soldas do Aço Inoxidável Lean Duplex UNS S32304 Utilizando Modelos de Encruamento. Thesis (Doctorate in Mechanical Engineering), Postgraduate Program in Mechanical Engineering, Federal University of Espírito Santo, Brazil, 2023;

[8] LIPPOLD, J.C.; KOTECKI, D.J. Welding Metallurgy and Weldability of Stainless Steels. [S.l.]: John Wiley & Sons, 2005;

[9] MOKHTARI, M.; POMMIER, P.; BALCAEN, Y.; ALEXIS, J. Laser Welding of AISI 316L Stainless Steel Produced by Additive Manufacturing or by Conventional Processes. J. Manuf. Mater. Process., v. 5, p. 136, 2021. DOI: https://doi.org/10.3390/jmmp5040136;

[10] YILBAS, B.S.; AKHTAR, S. Laser Welding of AISI 316 Steel: Microstructural and Stress Analysis. J. Manuf. Sci. Eng., 135, 031018, 2013. DOI: 10.1115/1.4024155;

[11] JIANG, M.; TAO, W.; CHEN, Y. Laser Welding under Vacuum: A Review. Applied sciences, v. 7, n. 9, p. 909, 2017;

[12] ARAUJO, O.; MACHADO, A.; OLIVEIRA, D.; LOPES, R. Enhancement of microCT images of steel cracks using mathematical filters. 10th Conference on Industrial Computed Tomography, Wels, Austria (iCT 2020), 2020. DOI: https://doi.org/10.58286/25106;

[13] ALVES, H.; FIRMINO, J.; CAVICHINI, A.; ORLANDO, M.; TADEU, R. Synthesis and characterization of metal-ceramic composite 316l/sycro. 9th Conference on Industrial Computed Tomography, Padova, Italy (iCT 2019), 2019. DOI: https://doi.org/10.58286/23678;

[14] SALUSTRE, M. G. et el. Study of steel matrix composite samples with 12%Wt TiB2 produced by spark plasma sintering. Materials Chemistry and Physics, 302, 127736, 2023. DOI: https://doi.org/10.1016/j.matchemphys.2023.127736.